2nd International Conference on Engineering Optimization
September 6-9, 2010, Lisbon, Portugal

Comparative Analysis of Commercial Aircraft Trajectory Performance

Manuel Soler*, Daniel Zapata[&], Alberto Olivares*, Ernesto Staffetti* and Jesús Cegarra[&]

*Universidad Rey Juan Carlos; Department of Statistics and Operations Research, Móstoles Madrid, Spain.
[&]GMV Aerospace and Defence; Department of Aeronautical Systems, Tres Cantos, Madrid, Spain.

Abstract
A hybrid optimal control approach to commercial aircraft trajectory optimization is proposed and tested comparing its results with short and medium-range typical flights. Given the sequence of phases and flight modes conforming the vertical flight profile of a commercial aircraft, the initial and final states and a set of path constraints, we solve the problem of finding control inputs, switching times between flight modes and the corresponding trajectory of the aircraft that minimizes fuel consumption. Three different profiles are defined for both ranges: typical nowadays flown profiles; free-flight profiles, used as optimal benchmark performance; and optimized procedure profiles. Performances, procedures and consumptions are analyzed. Results show that current flight profiles efficiency could be substantially improved seeking a new Air Trafic Management paradigm.
Keywords: Air traffic Management; Aircraft Trajectory Optimization; Hybrid Optimal Control.

1. Introduction

Air Traffic Management (ATM) is nowadays a very complex and highly regulated system that encompasses Air Traffic Flow Management (ATFM), Air Traffic Control (ATC) and AirSpace Management (ASM). A substantial change in the current ATM paradigm is needed because this system, which is responsible for sustainable, efficient and safe operations in civil aviation, is reaching the limit of its capabilities. Its capacity, efficiency, environmental impact and flexibility should be improved to accommodate airspace users requirements*. The need to fit aircraft trajectories to ATM system requirements makes them difficult to be optimized and, therefore, generally suboptimal flight profiles are being flown. This results in higher operative costs and higher emissions due to non minimal fuel consumption. Air traffic is responsible for 2% of CO_2 global emissions. Thus, minimizing both fuel consumption and emissions are interesting and challenging research subjects. Within the main goals of SESAR, i.e, 3-fold increase in air traffic movements whilst reducing delays; improve the safety performance by a factor of 10; 10% reduction in the effects aircraft have on the environment; provide ATM services at a cost to airspace users which at least 50% less, 4D trajectory shaping and optimization plays an important role for the concept of Trajectory Based Operations (TBO). Therefore, in this paper we focus on commercial aircraft minimum-fuel trajectory optimization towards a future, more flexible ATM concept of operation, meeting safety, effciency, cost effectiveness and environmental sustainability requirements in flight profiles.

With this aim, this paper presents an extension of [1], a hybrid approach to commercial aircraft optimal trajectory generation where different flight phases and operational procedures can be combined so that a single optimal control problem is solved. The coupling of these discrete flight phases with the continuous aircraft dynamics results in a hybrid system [2, 3, 4, 5]. In particular the flight of an aircraft has intrinsically got the characteristics of a controlled switched dynamical system [6, 7]. Indeed, several flight modes can be distinguished for climbing, cruising and descent, each with an associated dynamic model and a set of path constraints.

On the whole, it is difficult to find all the components for the solution to hybrid optimal control problems because the optimal sequence of discrete states is very difficult to determine. In our case, the phase sequence is given, but optimal switching times must be determined. Problems with known phase sequence have been frequently solved in aerospace engineering as multi-phase problems [8, 9, 10, 11], most of them were solved using pseudospectral methods [12, 13]. However, none of these works focused on commercial aircraft. Pseudospectral knotting methods have been developed for solving multiphase optimal control problems, see for instance [14]. Such knotting methods need knotting conditions to connect adjacent phases. In our approach we convert the hybrid optimal control into an equivalent, conventional optimal control problem, making the unknown switching times part of the state by using a method similar to those presented in [15, 16]. In this way, we do not need to connect adjacent phases with linkage constraints. The resulting optimal control problem is then solved using a Simpson collocation method [17, 18].

*SESAR ATM Master Plan: http://www.eurocontrol.int/sesar

The fundamental prior research work on aircraft trajectory optimization within the current ATM concept was presented in [19]. The flight of an aircraft was modelled as a collection of phases and procedures where continuity of the state variables was imposed in order to link phases, permitting discontinuities in control variables and flight path angle. Moreover, concatenating optimal phase-by-phase solutions does not lead to an overall optimal trajectory. A method to compute overall optimal trajectories was presented in [20]. Modelling the current ATM paradigm, as in [20], enforces the specification of two operative procedures per phase, for instance, to climb with constant V_{CAS} and constant throttle setting, or to perform a steady cruise, i.e., with constant Mach and constant altitude.

On the contrary, many works not based on the current ATM concept has been released: Some focused on minimizing fuel consumption only during aircraft cruise, e.g., [21], [22] and [23]. In [23] the interplay between aircraft mass and speed at constant altitude was studied to minimize fuel consumption, and important fuel savings were obtained when compared to steady cruise. The descent phase has also been widely studied, with special focus on Continuous Descent Approach (CDA), obtaining important fuel savings when putting it into practice in real scenarios [24, 25, 26, 27, 28, 29]. However, these results do not consider the fact that cruise or descent are just one of the different phases of a complete flight and therefore, they are not realistic because the optimal solution could significantly differ if we take into account the influence of previous and following phases.

In this work, an application to the method presented in [1] is reported. An optimized procedure flight, a free flight and a typical flight are compared in both a short-range flight and a medium-range flight scenarios. The results and performances are analyzed showing that important fuel savings could be achieved using the above mentioned approach.

2. The Hybrid Optimal Control Problem

The flight of an aircraft has intrinsically got the characteristics of a controlled switched dynamical system. Switched dynamical systems are particular cases of hybrid systems whose states is not subjected to discontinuous jumps.

A switched dynamical system is composed of a set of dynamic systems,

$$\dot{x} = f_k[x(t), u(t), t], k \in \{1, 2, \ldots, N_D\}, \tag{1}$$

where x represent the n-dimensional state vector, and the set $\{1, 2, \ldots, N_D\}$ represents the different dynamical systems, and a switching sequence in $[t_I, t_F]$, defined as the timed sequence of $N + 1$ active dynamical systems,

$$\sigma = [(t_I, k_I), (t_1, k_1), \ldots, (t_N, k_N)], \tag{2}$$

where $0 \leq N < \infty$, $t_I \leq t_1 \cdots \leq t_N \leq t_F$ and $k_j \in \{1, 2, \ldots, N_D\}$.

In order to control a switched dynamical system, both a m-dimensional control input, $u(t)$, and a switching sequence, σ, have to be specified. We suppose that the set of admissible control inputs is a set of piecewise continuous functions in $t \in [t_I, t_F]$. In this sequence, the pair (t_j, k_j) indicates that at time t_j the dynamic equation of the switched system changes from k_{j-1} to k_j, being $t_0 = t_I$ and $t_{N+1} = t_F$. As a consequence, in the time interval $[t_j, t_{j+1})$ the system evolution is governed by the dynamic equation k_j. In the interval $[t_N, t_F]$ the active dynamic system is k_N.

The pairs (t_j, k_j) can be classified in two categories: those corresponding to autonomous switches; and those corresponding to controlled switches. For instance, an autonomous switch may occur when the aircraft reaches a prescribed altitude. On the contrary, a controlled switch takes place in response to control inputs established by the solution to the optimal control problem. In this work, we assume that the sequence of phases is given by a flight profile, i.e., the untimed sequence of active systems $\zeta = (k_I, k_1, \ldots, k_N)$ is known.

The hybrid optimal control problem can be stated as follows: Consider the switched dynamic system (1) whose state and control variables are subjected to a set of equality and inequality constraints

$$g_k[x(t), u(t), t] = 0, h_k[x(t), u(t), t] \leq 0, k \in \{1, 2, \ldots, N_D\}. \tag{3}$$

Given an initial state, $x(t_I)$, a final state, $x(t_F)$, a time interval, $[t_I, t_F]$, and a prescribed untimed sequence of active dynamic systems, ζ, find a piecewise continuous input, $u(t)$, the switching instants, $(t_1, \ldots, t_N)$, and the corresponding piecewise smooth trajectory, $x(t)$, between $x(t_I)$ and $x(t_F)$ that fulfil (1), (3), and minimize

$$J = \phi[x(t_F)] + \int_{t_I}^{t_F} L[x(t), u(t), t]dt. \tag{4}$$

The final time, t_F, may be fixed or left free. We assume that f_k, g_k, h_k and ϕ are smooth enough functions.

This hybrid optimal control problem is converted into an optimal control problem, making the unknown switching times part of the state and introducing a new independent variable with respect to which the switching times are fixed [15, 16]. In this reformulated problem, there is a linear relation between the new variable and time, but the slope of this linear relation changes on each interval between two switches. These slopes, which are part of the solution to the optimal control problem, are actually time scaling factors that determine the optimal switching times. See Figure 1.

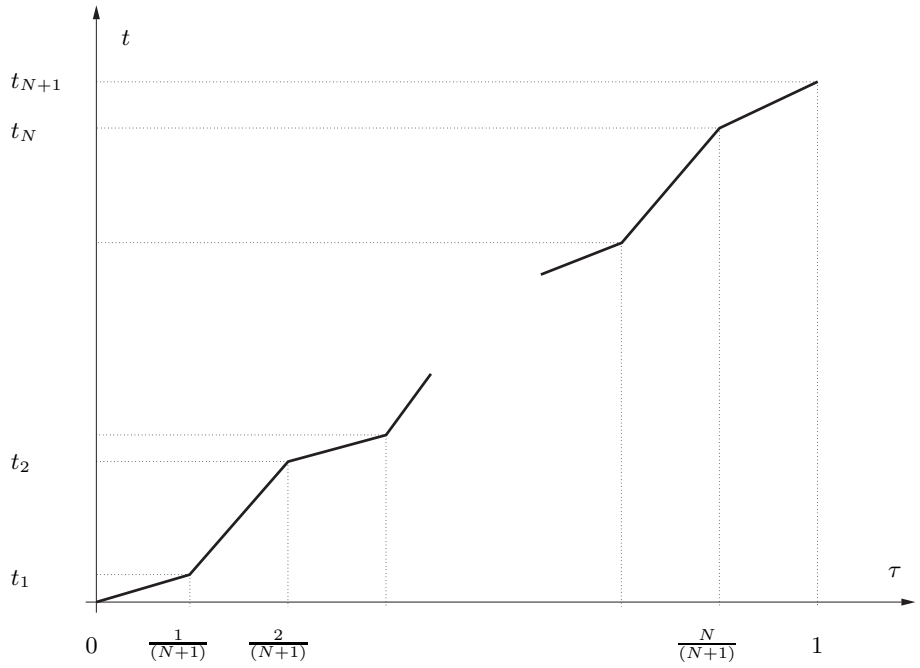

Figure 1: Relation between scaled time, τ, and real (unscaled) time t.

As previously stated, the number of switches, N, and the sequence of discrete states, ζ, which the system evolves through, are known. Without loss of generality, we can assume that $t_I = t_0 = 0$ and $t_F = t_{N+1} = 1$. The first step is to introduce the new state variables, $x_{n+1}, \ldots, x_{n+N}$, which correspond to the switching times, t_i, $i \in \{1, 2, \ldots, N\}$ i.e., $x_{n+i} = t_i$, with $\dot{x}_{n+i} = 0$.

We then introduce the new independent variable, τ. The relation between τ and t changes on each interval $[t_i, t_{i+1}]$. We establish piecewise linear correspondence between time, t, and the new independent variable, τ, so that for every chosen fixed point, τ_i, $i = 1, \ldots, N$, t equals t_i. Any monotonically increasing sequence of N numbers on interval $[0, 1]$ could be used. We set $\tau_i = i/(N+1)$. As a result we obtain the following expression

$$t = \begin{cases} (N+1)x_{n+1}\tau, & 0 \le \tau \le \frac{1}{N+1} \\ \ldots & \\ (N+1)(x_{n+i+1} - x_{n+i})\tau + (i+1)x_{n+i} - ix_{n+i+1}, & \frac{i}{N+1} < \tau \le \frac{i+1}{N+1} \\ \ldots & \\ (N+1)(1 - x_{n+N})\tau + (N+1)x_{n+N} - N, & \frac{N}{N+1} < \tau \le 1 \end{cases}$$

By introducing the new independent variable, τ, the evolution equation on the interval $[t_i, t_{i+1}]$ given by Equation (1) becomes

$$x' = (N+1)(x_{n+i+1} - x_{n+i})\hat{f}_i(x, u, \tau), \tag{5}$$

where $(\cdot)'$ denotes the derivative of $(\cdot)$ with respect to the new independent variable, τ, and

$$\hat{f}_i(x, u, \tau) = f_i(x, u, t(\tau)).$$

Let $\hat{x}$ be the extended state vector

$$\hat{x} = [x_1, \ldots, x_n, x_{n+1}, \ldots, x_{n+N}]^T,$$

Then, define on each interval $\frac{i}{N+1} < \tau \leq \frac{i+1}{N+1}$

$$\hat{L}(\hat{x}, u, \tau) = (N+1)(x_{n+i+1} - x_{n+i})L(x, u, t(\tau)).$$

We can rewrite the functional (4) as

$$\hat{J} \;=\; \phi\left(\hat{x}(1)\right) + \int_0^{\frac{1}{N+1}} \hat{L}(\hat{x}, u, \tau)d\tau + \cdots + \int_{\frac{N}{N+1}}^{1} \hat{L}(\hat{x}, u, \tau)d\tau \;=\; \phi\left(\hat{x}(1)\right) + \int_0^1 \hat{L}(\hat{x}, u, \tau)d\tau, \quad (6)$$

and the task is to minimize $\hat{J}$ in the extended state space, subject to the parameterized system given in (5), and to the corresponding path constraints in (3). The new equivalent problem is a conventional optimal control problem. The last N components of the optimal solution of this problem, $\hat{x}^*$, will be the optimal switching times $t_i, i = 1, \ldots, N$.

3. Cases study

The above exposed approach to hybrid optimal control problems (the reader is referred to [1] for more details) is herein tested comparing it with short-range and medium-range real flights. Typical, optimized and free-flight A320 vertical profiles are defined for both short and medium-range flights.

Free-flight profiles are defined modeling some restrictions due to airports terminal area operations together with an en-route free flight performance. Optimal performances are derived from such a profile seeking a future Trajectory Based Operations paradigm of ATM . The optimized procedure flight is nothing more than the overall-best-fit adjustment of the free flight to the imposed procedures; it is defined seeking a more efficient use of nowadays ATM paradigm. On the other hand, typical profiles have been defined strictly according to typical vertical profiles nowadays being flown.

3.1. Aircraft equiations of motion

We consider a 3 Degree Of Freedom (DOF) dynamic model that describes the point variable-mass motion of the aircraft over a flat Earth model. We consider the vertical motion of the aircraft. A standard atmosphere is defined with $\Delta T_{ISA} = 0$. C_L is, in general, a function of the angle of attack and the Mach number, i.e., $C_L = C_L(\alpha, M)$. The lift coefficient is used as a variable rather than the angle of attack. We assume a parabolic drag polar, i.e., $C_D = C_{D_0} + KC_L^2$. BADA 3.6[†] is used as aircraft performance models.

These hypotheses lead to the following set of ODEs for aircraft performance

$$\begin{aligned} m\dot{V} &= T - D - mg\sin\gamma, \\ mV\dot{\gamma} &= L - mg\cos\gamma, \\ \dot{x} &= V\cos\gamma, \\ \dot{h} &= V\sin\gamma, \\ \dot{m} &= -\eta T, \end{aligned} \quad (7)$$

where T and C_L are the control inputs and V, x, h, γ and m are the state variables.

Given a commercial flight profile as a sequence of phases, initial and final conditions, and a set of path constraints, our goal is to find the minimum-fuel consumption trajectory of the aircraft. Optimal switching times between phases and total flight time are also to be determined.

The characteristics of an Airbus A-320 have been taken from the BADA 3.6 database. The different aerodynamic configurations and the value of aerodynamic parameters are listed in Table 1.

The path constraints of the problem are those that conform the aircraft's flight envelope and have been taken from the BADA database manual [31]. CL_{max_i} and V_{Stall_i}, for $i = 1, \ldots, N$, vary depending on the aerodynamic

[†] http://www.eurocontrol.int

Table 1: A-320 Aerodynamic Configurations

Configuration	Flap	$C_{L_{max}}$	CD_0	K
TO	1+F	2.43	0.0393	0.0396
IC	1	2.19	0.0242	0.0469
CR	Clean	1.50	0.024	0.0375
AP	2	2.76	0.0456	0.0381
LD	Full	3.09	0.0838	0.0371

configuration. The rest of constraints are equal for all phases

$$\begin{aligned} &0 \leq h \leq \min[h_{M0}, h_u], && C_{V_{min}} V_{stall_i} \leq V \leq V_{Mo}, \\ &M \leq M_{M0}, && m_{min} \leq m \leq m_{max}, \\ &0 \leq C_L \leq C_{L_{max_i}}, && T \leq T_{max}, \\ &\dot{m}_{min} \leq \dot{m}, \end{aligned} \tag{8}$$

where $h_u = h_{max} + G_t(\Delta T_{ISA} - C_{Tc,4}) + G_W(m_{max} - m)$, and $C_{V_{min}} = 1.3$ (except for TO, where $C_{V_{min}} = 1.2$). Current Instrumental Landing Systems (ILS) set the constant descent path between -2.5 [deg] and -3.5 [deg], generally -3 [deg]. Therefore, regarding the landing phase, γ has also been constrained according to the typical values of an aircraft's final descent path, but also leaving some room for optimization, i.e.,

$$-6\ [deg] \leq \gamma_{Landing} \leq -2\ [deg]. \tag{9}$$

The reformulated optimal control problem is stated as follows

$$\min J = \int_0^{\frac{1}{N+1}} \hat{L}(\hat{x}, u, \tau) d\tau + \cdots + \int_{\frac{N}{N+1}}^1 \hat{L}(\hat{x}, u, \tau) d\tau \tag{10}$$

Subject to

$$x' = (N+1)(x_{n+i+1} - x_{n+i}) \hat{f}_i(x, u, \tau), \text{ dynamic constraint,} \tag{11}$$

$$x'_{n+1} = \ldots = x'_{n+N} = 0, \text{ switching dynamic constraint,} \tag{12}$$

$$x(t_I) = x_{t_I}, \text{ initial-boundary condition,} \tag{13}$$

$$\psi(x(t_F), t_F) = 0, \text{ final-boundary condition,} \tag{14}$$

$$\phi_{l_i} \leq \phi_i[x, u] \leq \phi_{u_i}, \text{ path constraints,} \tag{15}$$

where $i = 1, \ldots, N+1$ corresponds to the sequence of phases of the flight given in Table 1, N is the number of switches and $\hat{L}(\hat{x}, u, \tau) = m'$. Equation (11) corresponds to the aircraft ODE system given in (7), parametrized and particularized to the dynamic mode of each phase. Equation (12) are dynamical constraints associated to the switching variables. Equations (11) and (12) constitute the ODE system for the extended vector $\hat{x}$ and (13) and (14) are the initial and final conditions. Finally, (15) correspond to the set of constraints of each phase given in (8) and (9).

Both optimized and flight profiles are stated as hybrid optimal control problems. To solve the reformulated optimal control problem (10)-(15) a Simpson collocation method [17, 18] has been used. The resulting sparse nonlinear programming problem (NLP), has been solved using IPOPT [30]. Constraint (9) only apply for optimized profiles; free-flights profiles do not have a specific constraint in the landing phase regarding γ.

The typical profiles computation has been performed with a tool combining 3-DoF flight dynamics differential equations with procedure-oriented flight control. More precisely, the aircraft Ordinary Differential Equation (ODE) system (7) with the same performance and atmosphere models is integrated using the same set of path constraints (8), while controls are properly set so that the aircraft follows the given flight procedures.

3.2. Short range profile

Table 2, Table 3 and Table 4 show, respectively, the typical, optimized and free flight procedures used herein for the numerical simulation. The short range typical flight has been derived from a real Madrid-Oviedo flight plan following BADA-like flight procedure with airline-defined speed and altitude profile values.

The boundary conditions of the flight are the following: $x_{t_I} = 0$, $h_{t_I} = 0$, $v_{t_I} = 1.2V_{stall_{TO}}$ [m/s], $\gamma_{t_I} = 0.05$ [rad], $m_{t_I} = 63070$ [Kg]; $x_{t_F} = 476$ [km], $h_{t_F} = 0$.

Table 2: Short-Range Typical Flight Profile

Phase	Name	Configuration	End Trigger	Procedure	Op. Constraint
1	Take Off	TO	$V = 1.3V_{stall_{IC}}$	$T = T_{max}$	$V_{CAS} < 250kt$
2	Initial Climb	IC	$V = 1.3V_{stall_{CR}}$	$T = T_{max}$	$V_{CAS} < 250kt$
3	Res. Free Climb	CR	$h = 10000ft$	$T = T_{max}$	$V_{CAS} < 250kt$
4	Climb Accel	CR	$V_{CAS} = 300kt$	$h = 10000ft \& T = T_{max}$	
5	Climb CAS	CR	$Mach = 0.78$	$V_{CAS} = 300kt \& T = T_{max}$	
6	Climb Mach	CR	$h = FL320$	$Mach = 0.78 \& T = T_{max}$	
7	Cruise	CR	-	$h = FL320 \& Mach = 0.78$	
8	Descent Mach	CR	$V_{CAS} = 300kt$	$Mach = 0.78 \& T_{min}$	
9	Descent CAS	CR	$h = 10000ft$	$V_{CAS} = 300kt \& T_{min}$	
10	Descent Decel	CR	$V_{CAS} = 250kt$	$h = 10000ft \& T_{min}$	
11	Res. Free Descent	CR	$h = 6000ft$	T_{min}	$V_{CAS} < 250kt$
12	Approach	AP	$h = 2000ft.$	$\gamma = -3$	$V_{CAS} < 250kt$
13	Landing	LD	Final cond.	$\gamma = -3$	$V_{CAS} < 250kt$

Table 3: Short-Range Optimized Procedure Flight Profile

Phase	Name	Configuration	End Trigger	Procedure	Op. Constraint
1	Take Off	TO	$V = 1.3V_{stall_{IC}}$	Free	$V_{CAS} < 250kt$
2	Initial Climb	IC	$V = 1.3V_{stall_{CR}}$	Free	$V_{CAS} < 250kt$
3	Res. Free Climb	CR	$h = 10000ft$	Free	$V_{CAS} < 250kt$
4	Climb Accel	CR	-	$h = 10000ft$	
5	Climb CAS	CR	-	$V_{CAS} = c_1 \& T = T_{max}$	
6	Climb Mach	CR	-	$Mach = c_2 \& T = T_{max}$	
7	Cruise	CR	-	$h = c_3$	
8	Descent Mach	CR	-	$Mach = c_4$	
9	Descent CAS	CR	$h = 10000ft$	$V_{CAS} = c_5$	
10	Descent Decel	CR	-	$h = 10000ft$	
11	Res. Free Descent	CR	$h = 6000ft$	T_{min}	$V_{CAS} < 250kt$
12	Approach	AP	$h = 2000ft.$	$\gamma = c_6$	$V_{CAS} < 250kt$
13	Landing	LD	Final cond.	$\gamma = c_6$	$V_{CAS} < 250kt$

* Being $c_1, \ldots, c_6$ constant values to be determined by the optimal solution of the problem.

Table 4: Short-Range Free Flight Profile

Phase	Name	Configuration	End Trigger	Procedure	Op. Constraint
1	Take Off	TO	$V = 1.3V_{stall_{IC}}$	Free	$V_{CAS} < 250kt$
2	Initial Climb	IC	$V = 1.3V_{stall_{CR}}$	Free	$V_{CAS} < 250kt$
3	Res. Free Climb	CR	$h = 10000ft$	Free	$V_{CAS} < 250kt$
4	Free CL/CR/DS	CR	$h = 10000ft$	Free	
5	Res. Free Descent	CR	$h = 6000ft$	Free	$V_{CAS} < 250kt$
6	Approach	AP	$h = 2000ft.$	Free	$V_{CAS} < 250kt$
7	Landing	LD	Final cond.	Free	$V_{CAS} < 250kt$

3.3. Medium range profile

Table 5, Table 6 and Table 7 show, respectively, the typical, optimized and free flight procedures used herein for the numerical simulation. The medium range typical flight has been derived from a real Madrid-Berlin flight plan following BADA-like flight procedure with airline-defined speed and altitude profile values.

The boundary conditions of the flight are the following: $x_{t_I} = 0$, $h_{t_I} = 0$, $v_{t_I} = 1.2V_{stall_{TO}}$ [m/s], $\gamma_{t_I} = 0.05$ [rad], $m_{t_I} = 69415$ [Kg]; $x_{t_F} = 2035$ [km], $h_{t_F} = 0$.

Table 5: Medium-Range Typical Flight Profile

Phase	Name	Configuration	End Trigger	Procedure	Op. Constraint
1	Take Off	TO	$V = 1.3V_{stall_{IC}}$	$T = T_{max}$	$V_{CAS} < 250kt$
2	Initial Climb	IC	$V = 1.3V_{stall_{CR}}$	$T = T_{max}$	$V_{CAS} < 250kt$
3	Res. Free Climb	CR	$h = 10000ft$	$T = T_{max}$	$V_{CAS} < 250kt$
4	Climb Accel	CR	$V_{CAS} = 300kt$	$h = 10000ft \& T = T_{max}$	
5	Climb CAS	CR	$Mach = 0.78$	$V_{CAS} = 300kt \& T = T_{max}$	
6	Climb Mach	CR	$h = FL360$	$Mach = 0.78 \& T = T_{max}$	
7	Cruise	CR	-	$h = FL360 \& Mach = 0.78$	
8	Descent Mach	CR	$V_{CAS} = 300kt$	$Mach = 0.78 \& T_{min}$	
9	Descent CAS	CR	h = 10000 ft	$V_{CAS} = 300kt \& T_{min}$	
10	Descent Decel	CR	$V_{CAS} = 250kt$	$h = 10000ft \& T_{min}$	
11	Res. Free Descent	CR	$h = 6000ft$	T_{min}	$V_{CAS} < 250kt$
12	Approach	AP	$h = 2000ft.$	$\gamma = -3$	$V_{CAS} < 250kt$
13	Landing	LD	Final cond.	$\gamma = -3$	$V_{CAS} < 250kt$

Table 6: Medium-Range Optimized Procedure Flight Profile

Phase	Name	Configuration	End Trigger	Procedure	Op. Constraint
1	Take Off	TO	$V = 1.3V_{stall_{IC}}$	Free	$V_{CAS} < 250kt$
2	Initial Climb	IC	$V = 1.3V_{stall_{CR}}$	Free	$V_{CAS} < 250kt$
3	Res. Free Climb	CR	$h = 10000ft$	Free	$V_{CAS} < 250kt$
4	Climb Accel	CR	-	$h = 10000ft$	
5	Climb CAS	CR	-	$V_{CAS} = c_1^* \& T = T_{max}$	
6	Climb Mach	CR	-	$Mach = c_2 \& T = T_{max}$	
7	Cruise	CR	-	$h = c_3$	
8	Descent Mach	CR	-	$Mach = c_4$	
9	Descent CAS	CR	$h = 10000ft$	$V_{CAS} = c_5$	
10	Descent Decel	CR	-	$h = 10000ft$	
11	Res. Free Descent	CR	$h = 6000ft$	T_{min}	$V_{CAS} < 250kt$
12	Approach	AP	$h = 2000ft.$	$\gamma = c_6$	$V_{CAS} < 250kt$
13	Landing	LD	Final cond.	$\gamma = c_6$	$V_{CAS} < 250kt$

* Being $c_1, \ldots, c_6$ constant values to be determined by the optimal solution of the problem.

Table 7: Medium-Range Free Flight Profile

Phase	Name	Configuration	End Trigger	Procedure	Op. Constraint
1	Take Off	TO	$V = 1.3V_{stall_{IC}}$	Free	$V_{CAS} < 250kt$
2	Initial Climb	IC	$V = 1.3V_{stall_{CR}}$	Free	$V_{CAS} < 250kt$
3	Res. Free Climb	CR	$h = 10000ft$	Free	$V_{CAS} < 250kt$
4	Free CL/CR/DS	CR	$h = 10000ft$	Free	
5	Res. Free Descent	CR	$h = 6000ft$	Free	$V_{CAS} < 250kt$
6	Approach	AP	$h = 2000ft.$	Free	$V_{CAS} < 250kt$
7	Landing	LD	Final cond.	Free	$V_{CAS} < 250kt$

4. Results

Tables 8 and 9, and Figures 2-5 show the results of the different simulations. Since optimized and free-flight profiles have been stated with the hybrid approach above explained, for the sake of clarity, optimal control law, optimal switching instants and the evolution of the state variables are represented in Figures 2-5 in terms of scaled time, τ, (ranging from 0 to 1) and in terms of real time, t. On the contrary, the typical profile is only depicted in terms of real time since neither scaled time nor switching times can be simulated within the used algorithm for typical profiles.

Regarding both short and medium optimized profiles, a discretization grid has been defined for τ with $n = 650$ ($n_1 = n_2 \dots n_{13} = 50$). Free flights are defined as well with a $n = 650$ grid in τ; in this case, for the sake of comparison, the 4th phase is composed by 350 discrete states, being the 3 previous and 3 following phases composed by 50 discrete states. Typical flights are computed in real times with samples every second. In Figures 2-5 the vertical dashed lines denote the transition between phases regarding just the optimized profile, so that the phases are clearly distinguishable in both timescales for the optimized case.

Referring the reader to Tables 2 and 7, it can be observed that the optimized profiles are defined with some trigger conditions, the so called capture conditions for switching. When this occur, the switchings are claimed as autonomous, e.g., they occur when the aircraft reaches the respective altitudes or velocities. On the contrary, switches between phases with non-capture conditions are claimed as controlled switches since they are given by the control law within the optimal solution. It is straight forward to see that the main difference between typical and optimized profiles is, together with less restricted procedures, the fact that some controlled switches are allowed. As a consequence, the transition Mach, the cruising altitude or the constant calibrated speed of descent are not pre-fixed, but are set by the optimal solution, leading the system to the overall minimum fuel consumption. The free flight herein proposed, indeed a "pseudo" free flight since Standard Instrument Departure (SID) and Standard Terminal Arrival Route (STAR) constraints must be model due terminal area restrictions, intend to model the best available performance. The optimized procedure flight is nothing more than the overall-best-fit adjustment of the free flight to the imposed procedures. Such en-route imposed procedures are derived from a better ATC and ATM performance instead of a pure en-route free flight.

To conclude this general remarks, note that for both medium and short range profiles free flights consumption is the lest with the longest duration. Optimized profiles achieve values in between but very close to those reached by free flights. It's remarkable that, though 13 phases are specified, the algorithm neglects those spurious ones; in this case the phases 8 and 10, descent Mach and Descent Deceleration, are dismissed by the optimal solution by setting the corresponding steps to zero, i.e., setting equal switching times. By this mean, the algorithm leads the aircraft to what would be a CDA.

4.1. Short Range

Table 8 shows the results regarding the short range profile: It contains the total flight time for the typical flight (Time [s] typ), 2592 [s]; the optimized profile 12 switching times between phases (Swit [s] opt) and the total flight time, 2922 [s]; The free flight profile 6 switches (Swit [s] free) and the final time, 2942 [s]; the final consumption of the typical profile (Con [kg] typ); the optimized profile accumulated consumption at the end of every phase (Con [kg] opt), being 1752 [Kg] the total consumption; the free-flight profile accumulated consumption at the end of every phase (Con [kg] free), being 1741 [Kg] the total consumption; the constant values that describe optimized aircraft performance in the different flight procedures (Value opt), which are indeed part of the optimal solution.

The optimal control law, the optimal switching instants and the evolution of the state variables are represented in Figures 2-3. Regarding the state variables, in general, except for the case of γ -Figure 3-, all state variables vary smoothly. γ exhibit high-frequency dynamics at some points near the switchings, but are within reasonable values for aircraft performance. Figure 4 shows the behavior of control inputs, where some bang-bang behavior can be observed in the evolution of thrust within the optimized 8th phase. Also C_L shows a high frequency behavior in this phase for the optimized case. Free flight controls show, however, a smooth behavior.

Regarding aircraft performances, result exhibit as well high concordance. The optimum free flight starts seeking to achieve maximum altitude in minimum time, since flying at low altitudes with maximum thrust setting is very fuel consuming. As the aircraft gets higher, it progressively softens its rate of climb until it suddenly performs a sharp climb maneuver to intercept the optimum descent path, thus skipping cruise phase. With this maneuver, the aircraft consumes the excess speed with respect to the optimum descent speed, while enabling an anticipated interception of the optimum descent path thanks to the fast altitude gain. Otherwise, the nominal climb would last longer, resulting in greater fuel consumption.

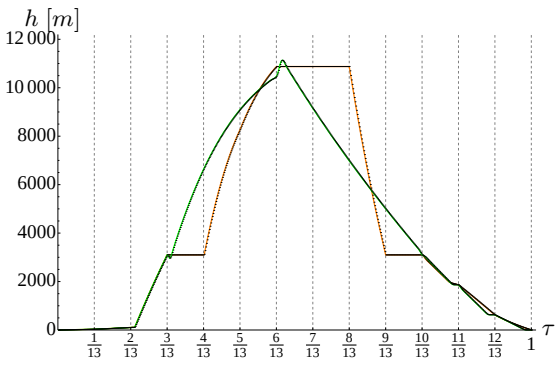

(a) τ-h

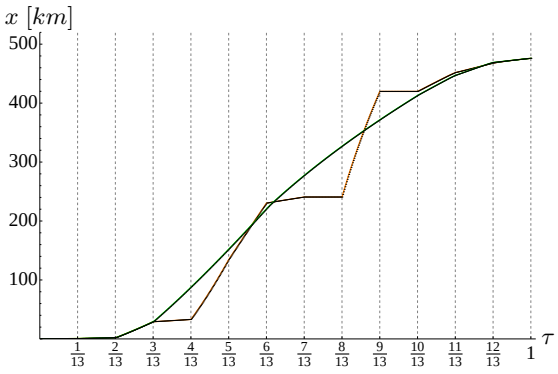

(b) τ-x

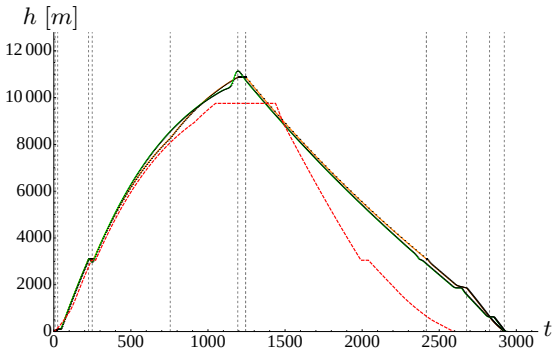

(c) t-h

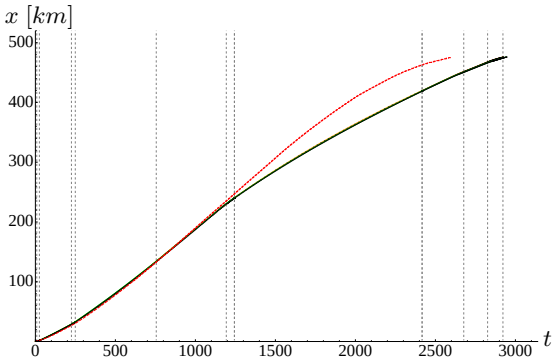

(d) t-x

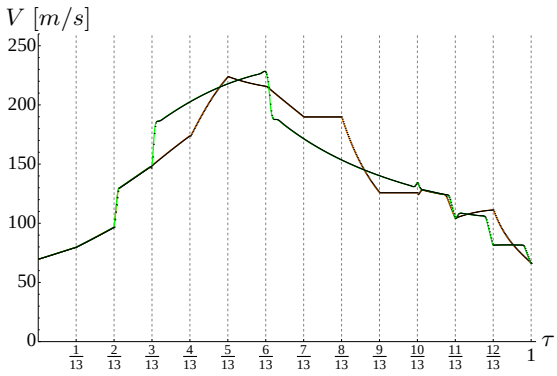

(e) τ-V

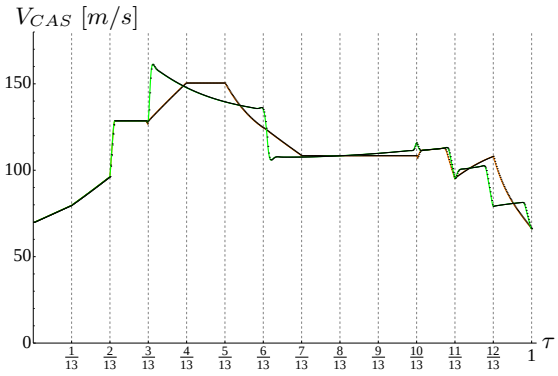

(f) τ-V_{CAS}

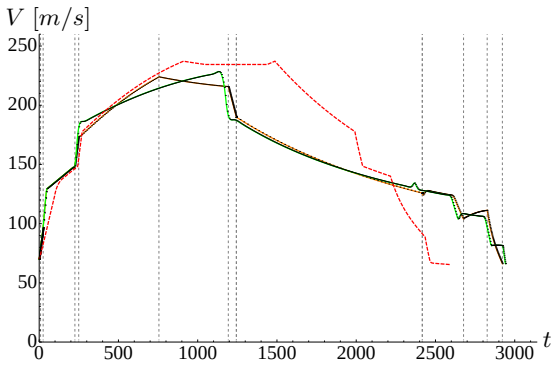

(g) t-V

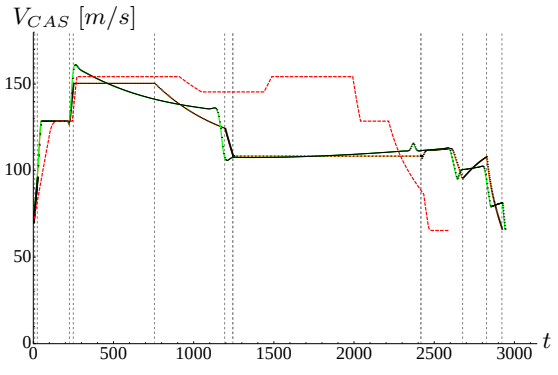

(h) t-V_{CAS}

Figure 2: Short range altitude, h, distance, x, True Air Speed, V, and Calibrated AirSpeed, V_{CAS}: dashed red line corresponds to typical profile -only depicted in real time charts since was not calculated with the hybrid approach-; solid dotted-orange line corresponds to optimized profile -being the dots the computed discrete states-; solid dotted-green corresponds to free-flight profile -being the dots the computed discrete states-. Note that the depicted vertical dashed lines in both timescales correspond to the optimized profile switching times.

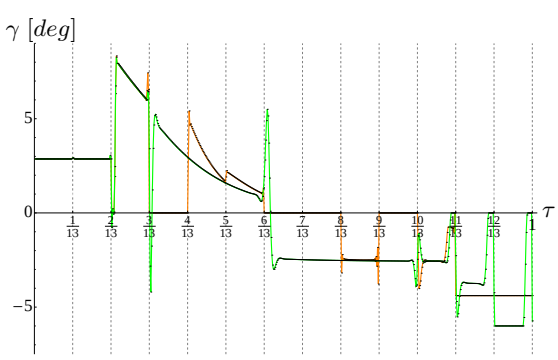

(a) τ-γ

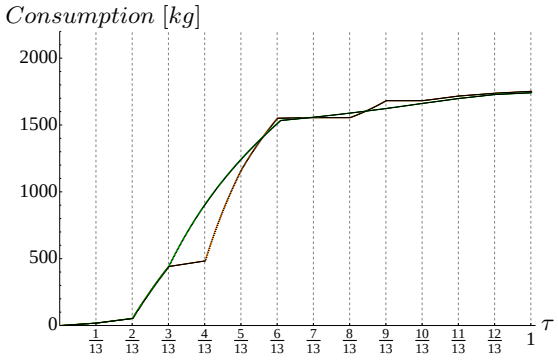

(b) τ-m

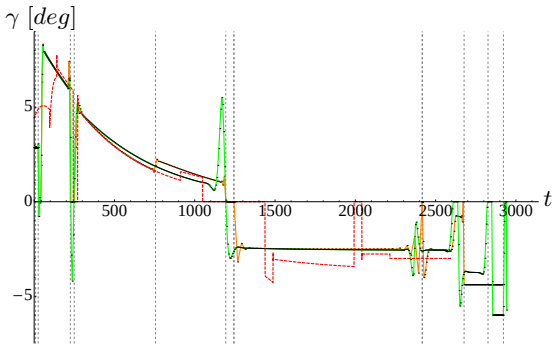

(c) t-γ

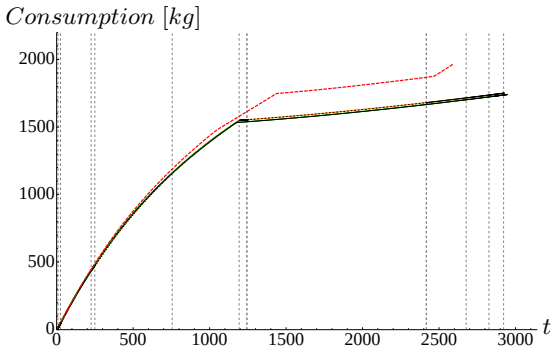

(d) t-m

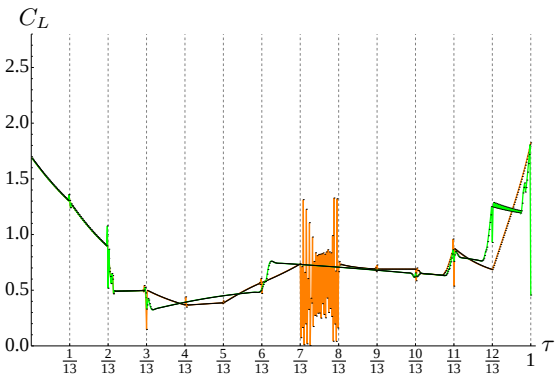

(e) τ-C_L

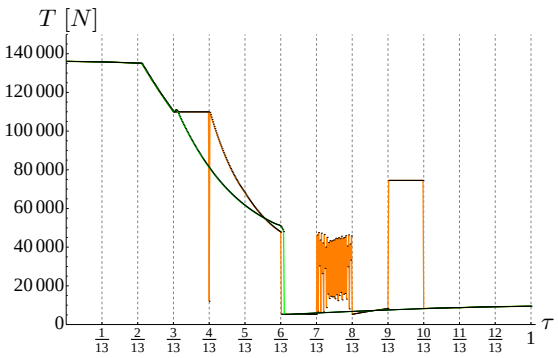

(f) τ-T

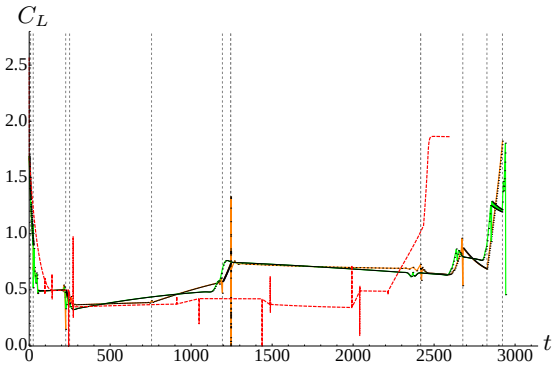

(g) t-C_L

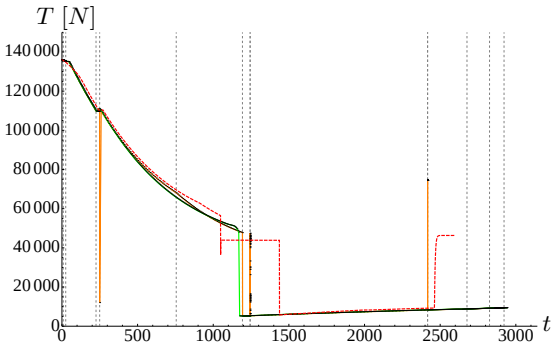

(h) t-T

Figure 3: Short range consumption, flight path angle, γ, and control laws, T & C_L : dashed red line corresponds to typical profile -only depicted in real time charts since was not calculated with the hybrid approach-; solid dotted-orange line corresponds to optimized profile -being the dots the computed discrete states-; solid dotted-green corresponds to free-flight profile -being the dots the computed discrete states-. Note that the depicted vertical dashed lines in both timescales correspond to the optimized profile switching times.

The optimum descent path is the result of descending at maximum gradient speed, which allows the aircraft to fly the greatest distance possible at idle thrust, thus minimizing fuel consumption. This optimum speed is the minimum drag speed, also known as base speed. This speed decreases as air density increases, so the aircraft lowers its speed as it descends. The base speed also changes as the aircraft deploys high-lift devices, so the aircraft speed is adjusted by regulating the flight path angle when a change in aerodynamic configuration is to be performed. At the very end of the flight, when the only aim is to land at any flyable speed, the flight path angle is increased to cover the greatest distance possible before touching ground, consuming the speed excess above minimum speed.

Table 8: short range results

Ph	Time [s] typ	Swit [s] opt	Swit [s] free*	Con [kg] typ	Con [kg] opt	Con [kg] free	Value opt
1	-	8.69	8.69	-	18.16	18.16	Free
2	-	25.04	25.06	-	52.94	52.96	Free
3	-	225.3	225.38	-	441.44	441.57	Free
4	-	249.41	-	-	482.71	-	$h = 10000ft$
5	-	755.409	-	-	1161.36	-	$V_{CAS} = 150.459$ & T_{max}
6	-	1193.11	-	-	1550.29	-	$Mach = 0.7297$ & T_{max}
7	-	1243.9	-	-	1554.87	-	$h = 10875.4$
8	-	1243.9	-	-	1554.87	-	$Mach = 0.6422$
9	-	2416.84	-	-	1681.77	-	$V_{CAS} = 108.406$
10	-	2416.84	2368.83	-	1681.77	1661.55	$h = 10000ft$
11	-	2677.17	2642.83	-	1716.68	1698.26	T_{min}
12	-	2826.22	2853.54	-	1737.66	1728.08	$\gamma = -4.3911$ [deg]
13	2592.8	2922.08	2942.26	1967.15	1752.71	1741.09	$\gamma = -4.3911$ [deg]

* Assuming that optimized phases number 4 to 9 correspond to free phase 4 and, consequently, Ph 10 corresponds to free 5th phase, etc.

There are two main differences when performing the descent between typical procedure flight and free flight. The first one is that typical flights descend at a speed much higher than the base speed (aprox 300kt vs 210kt). This permits typical flights to reduce flight duration at the cost of increasing fuel consumption. The second difference is that typical flights perform the approach at the ILS -3 glide path. When the approach glide path is less inclined than the maximum gradient path (as in this case), the glide path becomes too soft for the aircraft to maintain the desired speed at idle thrust. Thus, some extra thrust is required during the approach, resulting in increased fuel consumption.

The optimized flight tries always to follow the patterns of free flight optimal performance. Consequently, first it seems that the algorithm aims to minimize climb phase duration since it is very fuel consuming. But at the same time it needs to prevent negatively affecting the optimality of the subsequent flight phases. The selected 292[kt]/0.73 climb speed is similar to the typical profile in the constant CAS phase but shows a significantly lower speed for the constant Mach phase, probably because it provides an increased rate of climb. Then the aircraft performs a short cruise (4 [sec]), indeed such duration is just needed to decelerate from the climbing velocity to the descending one. Eventually the aircraft intercepts the descending path, performing it at 108 [m/s] (CAS), 211 [kt] aprox., considerable different than the typical 300 [kt]. This is optimal thanks to the minimum drag CAS being almost constant along the descent, consequently neglecting the constant Mach phase. Finally, the constant flight path angle of initial and final approach, -4.39 [deg], is more inclined than the typical one, -3 [deg] .

All this considerations clearly justify the fuel burning savings achieved, more than 200 [kg] . It is necessary to point out that BADA aerodynamic model does not take into account compressibility effects on the aerodynamic behaviour of the aircraft. This leads to lower-than-real drag at high mach numbers, resulting in higher-than-real optimum speeds and altitudes.

4.2. Medium Range

Table 9 shows the results regarding the medium range profile. For its interpretation, without loss of generality, stand the same as pointed out for the case of short range profile. The optimal control law, the optimal switching instants and the evolution of the state variables are represented in Figures 4-5. Without loss of generality, regarding the behavior of states and controls, all stated for the case of short range remains valid in medium range. Therefore the algorithm shows a predecible and rather smooth behavior in both states and controls.

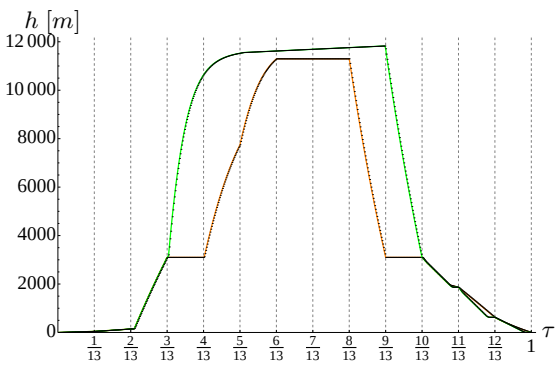

(a) τ-h

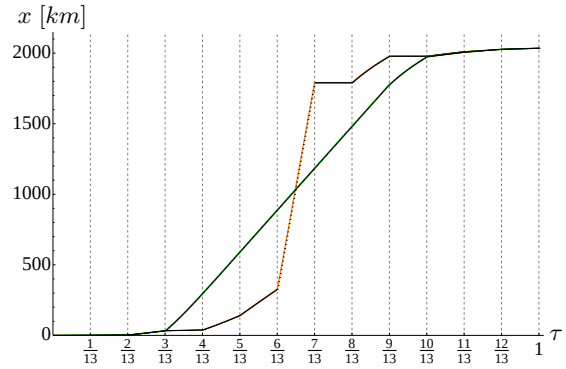

(b) τ-x

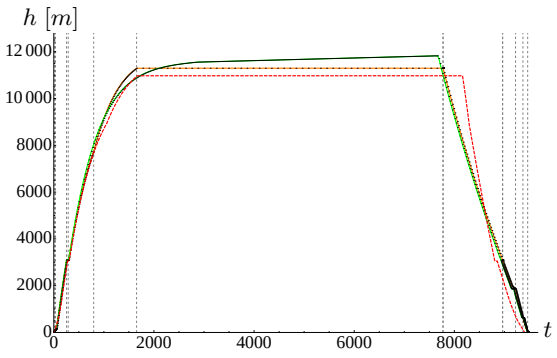

(c) t-h

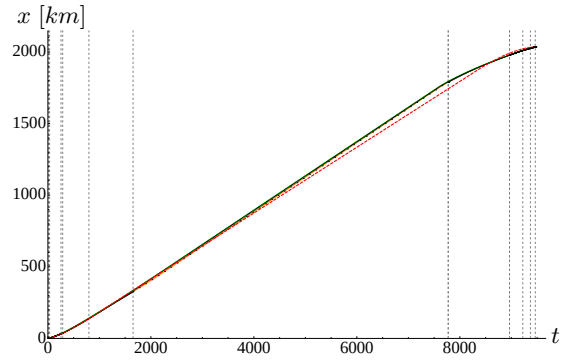

(d) t-x

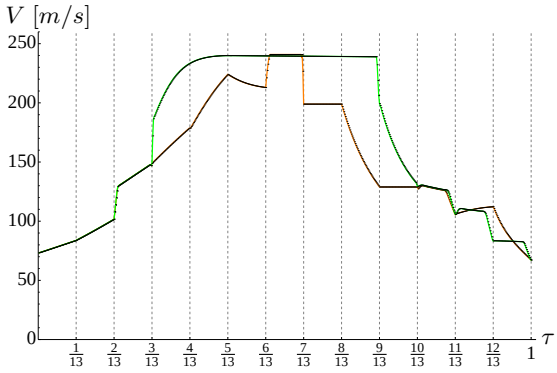

(e) τ-V

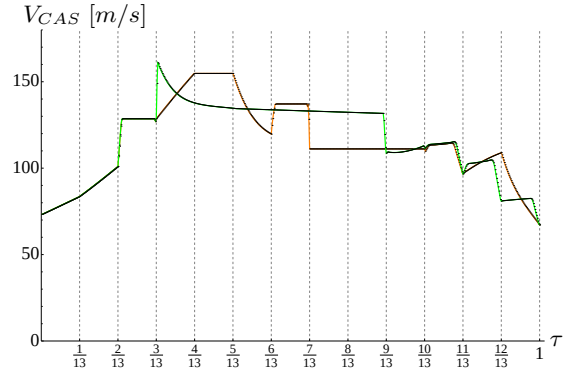

(f) τ-V_{CAS}

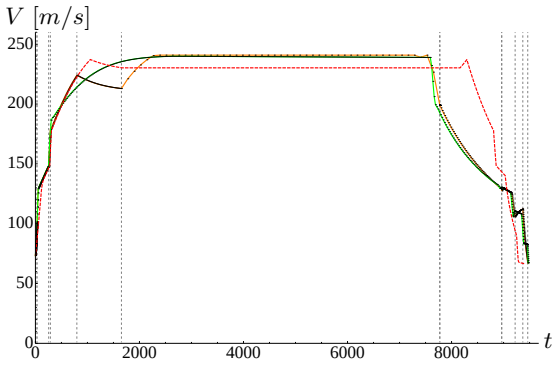

(g) t-V

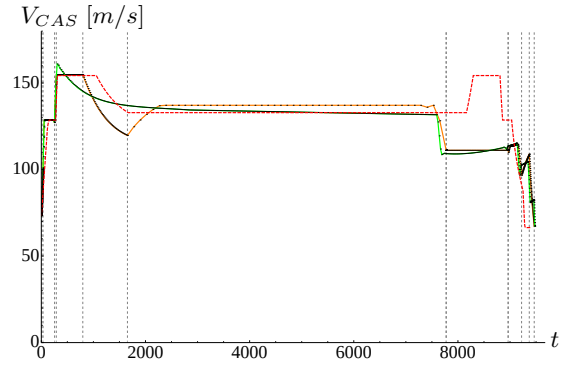

(h) t-V_{CAS}

Figure 4: Medium range altitude, h, distance, x, True Air Speed, V, and Calibrated AirSpeed, V_{CAS}: dashed red line corresponds to typical profile -only depicted in real time charts since was not calculated with the hybrid approach-; solid dotted-orange line corresponds to optimized profile -being the dots the computed discrete states-; solid dotted-green corresponds to free-flight profile -being the dots the computed discrete states-. Note that the depicted vertical dashed lines in both timescales correspond to the optimized profile switching times.

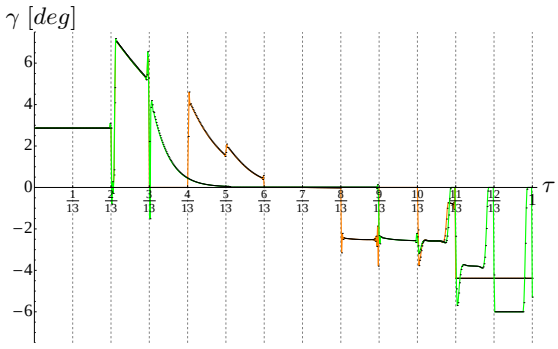

(a) τ-γ

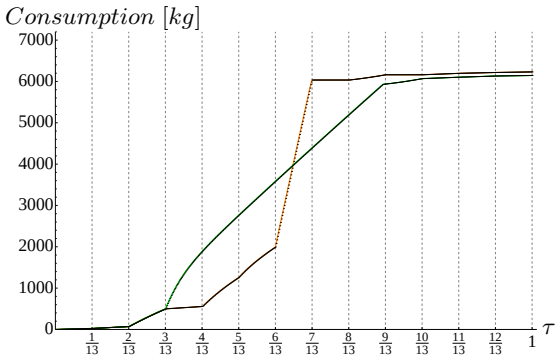

(b) τ-m

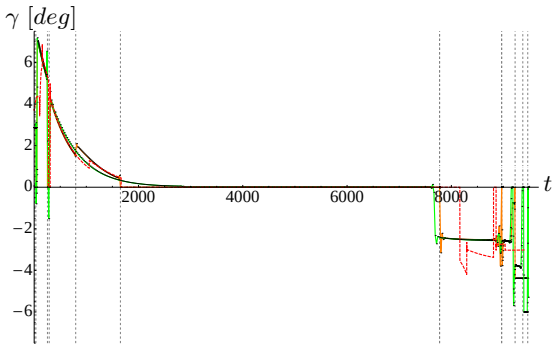

(c) t-γ

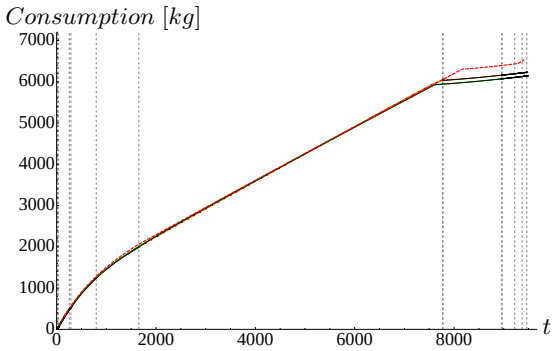

(d) t-m

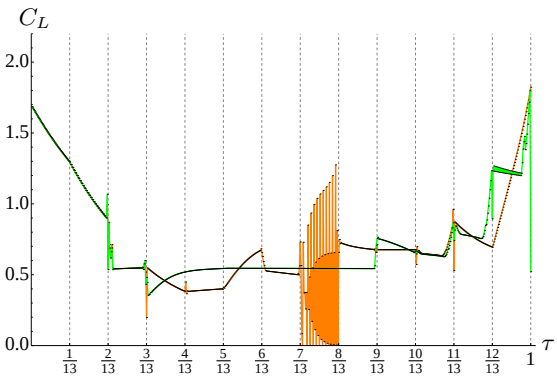

(e) τ-C_L

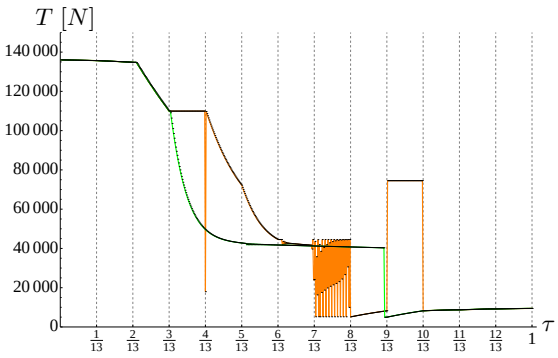

(f) τ-T

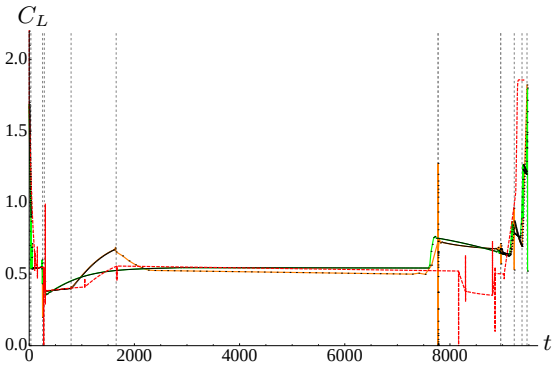

(g) t-C_L

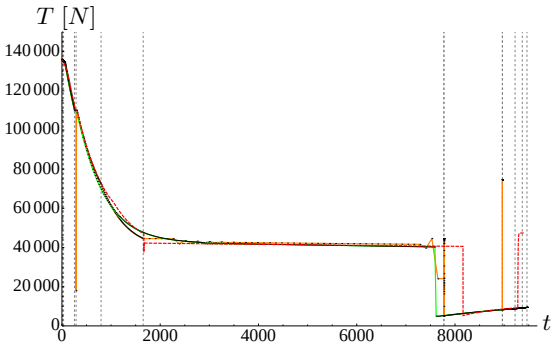

(h) t-T

Figure 5: Medium range consumption, flight path angle, γ, and control laws, T & C_L: dashed red line corresponds to typical profile -only depicted in real time charts since was not calculated with the hybrid approach-; solid dotted-orange line corresponds to optimized profile -being the dots the computed discrete states-; solid dotted-green corresponds to free-flight profile -being the dots the computed discrete states-. Note that the depicted vertical dashed lines in both timescales correspond to the optimized profile switching times.

The optimum free flight starts seeking to achieve maximum altitude in minimum time, since flying at low altitudes with maximum thrust setting is very fuel consuming. As the aircraft gets higher, it progressively softens its rate of climb to make a smooth transition to the subsequent pseudo-cruise phase, in which the aircraft asymptotically approaches its operating ceiling. The optimization target during cruise is to maximize the specific range, which is the distance traveled per unit of fuel consumed. As the aircraft mass decreases due to fuel burn, the optimum profile shows an increasing trend in altitude following the also-increasing operating ceiling, while speed is conveniently adjusted, typically in a slightly decreasing trend. Such a performance is known as continuous cruise climb. Cruise phase ends when the optimum descent path is intercepted. For the optimum descent path, without loss of generality, it states the principles of free optimal performance explained for short-range profiles.

Table 9: Medium range results

Ph	Swit [s] typ	Swit [s] opt	Swit [s] free	Con [kg] typ	Con [kg] opt	Con [kg] free	Value opt
1	-	11.61	11.61	-	24.26	24.26	Free
2	-	33.28	33.29	-	70.25	70.27	Free
3	-	254.66	254.71	-	498.50	498.58	Free
4	-	287.89	-	-	555.43	-	$h = 10000ft$
5	-	796.57	-	-	1258.31	-	$V_{CAS} = 154.817$ & T_{max}
6	-	1653.76	-	-	1995.43	-	$Mach = 0.7249$ & T_{max}
7	-	7774.07	-	-	6034.37	-	$h = 11295.4$
8	-	7774.08	-	-	6034.38	-	$Mach = 0.6772$
9	-	8964.12	-	-	6161.77	-	$V_{CAS} = 111.138$
10	-	8964.12	8929.65	-	6161.77	6068.77	$h = 10000ft$
11	-	9222.08	9184.45	-	6196.36	6102.95	T_{min}
12	-	9369.81	9388.6	-	6217.16	6131.87	$\gamma = -4.3823$ [deg]
13	9403.5	9464.6	9475.87	6529.85	6231.05	6144.66	$\gamma = -4.3823$ [deg]

Again, as pointed out for the short-range profile, the optimized flight tries always to follow the patterns of free flight optimal performance. Consequently, it seems that the algorithm aims to minimize climb phase duration since it is very fuel consuming. But at the same time it needs to prevent negatively affecting the optimality of the subsequent flight phases. The selected 301[kt]/0.72 climb speed is similar to the typical profile in the constant CAS phase but shows a significantly lower speed for the constant Mach phase, probably because it provides an increased rate of climb. Then the aircraft performs the cruise at an altitude that is not the instantaneous optimal but an overall suboptimal value limited by the operating ceiling at the beginning of cruise (where the ceiling is lower due to the greater mass). Eventually the aircraft intercepts the descending path, performing it at 111 [m/s] (CAS), 215 [kt] aprox., considerable different than the typical 300 [kt]. This is optimal thanks to the minimum drag CAS being almost constant along the descent, consequently neglecting the constant Mach phase. Finally, the constant flight path angle of initial and final approach, -4.38 [deg], is more inclined than the typical one, -3 [deg] . Again, the two main differences when performing free flight descent are clearly achieved in the optimized simulations.

All this considerations clearly justify the fuel burning savings achieved, almost 300 [kg] when comparing optimized with typical, and almost 400 [kg] when comparing free flight with typical. Notice that a closer performance to free flight's continuous cruise climb could have been achieved by defining at least one step climb. Again, it is necessary to point out that BADA aerodynamic model does not take into account compressibility effects on the aerodynamic behaviour of the aircraft. This leads to lower-than-real drag at high mach numbers, resulting in higher-than-real optimum speeds and altitudes.

5. Conclusions

This paper proposes a hybrid optimal control approach to commercial aircraft trajectory optimization, showing that gate to gate trajectory optimization could be address with such an approach. The proposed optimized-procedure profiles are tested by comparing them with typical flights, seeking fuel savings, and with free flights, analyzing how close are they from the theoretical optimal performance.

The key differences of performance arise in descent phases, where indeed descent velocity and ILS arrival flight path angle exhibit high deviations from what has been shown as optimal: to descent at base velocity and to perform approach and landing at maximum gradient path. There are also defined phases, such as Descent Mach and Descent Deceleration, that are clearly inefficient and thus spurious. A first conclusion is that the algorithm

showed robustness when dealing with such spurious phases and was capable to neglect them, leading to CDA optimal descent performance, even in the case we consider all previous phases. Indeed, the medium range cruise could be further optimized near to the fee-flight's continuous cruise climbing by simply adding a certain number of step climbs; the algorithm would then set the spurious ones to zero.

Assuming that profiles need to be restricted in departure and arrival terminal area, the free flight profiles herein exposed can be claimed as optimal performance benchmarks. Results show that both short and medium range free-flights profiles could achieve, respectively, 11.5% and 5.9% of fuel savings when compared to typical profiles. Furthermore, results also show that short and medium range optimized profiles could also save, respectively, 10.9% and 4.6% when compared to typical profiles. A second conclusion is that such this approach for optimized profiles provides a framework to plan flights with much less consumption than today's ones, indeed very close to what is suppose to be free-flight optimal performance, but also defining more trackable procedures, which will help ATM in defining a more efficient, sustainable new paradigm while maintaining safety operations.

Derived from that, a question arises: then, why are these vertical profiles not applied nowadays? Focusing on descent, we should consider separately the track going from the top of descent to the initial approach fix, and the track going from that fix to the runway. The first track could be improved without operational problems by just following the profile given by maximum gradient velocity at idle thrust. In lack of that, a constant CAS procedure around the average base velocity could be defined, which as it has been said is not far from the optimal. The main reason that current flights use a constant CAS up to 300 [kt] is probably to reduce descent duration. Regarding final and initial approach, it does not seem to be such easily achievable to perform the obtained results. Free flight optimal path shows a very steep path, while performing landing with quasi-level flight. This profile is problematic because descent path are designed as a trade off between obstacles handling and not excessive descent rates. Free flight shows rather a high descent rate followed by a potentially non-handling obstacles horizontal path. Optimized descent paths showed, however, higher than nowadays ILS constant path angles, closer to optimal path, avoiding also potential obstacles. Such a paths would lead to higher descent rates, but not such as free-flights descent paths. The paradigm of Global Navigation Satellite System (GNSS) descent procedures will help defining "ad hoc" descent paths within safety standards and thus, some of the above obtained fuel savings could be achieved. To combine both descent tracks would lead us to CDA. A much more complicated scenario of real application arises here since we must ensure non-collision and predefine the optimal sequence of aircrafts before the top of descent. Since optimized profiles seems more likely to be applied in short-term, or maybe a combination between free-flight descent and optimized approach and landing, a third conclusion is that the obtained fuel saving could be effectively obtained, at least the optimized profiles ones.

For further conclusions, a more realistic model must be taken into account, specifically considering compressibility at high Mach numbers. 3D dynamics, waypoints and overflight costs, emissions costs, or wind deterministic & stochastic models could be some extensions of this work. Regarding conflict resolution, in the time being it seems more likely to obtain one-by-one gate to gate optimal paths and then address "ad hoc" conflict resolution at every sector.

Acknowledgements

This work is partially supported by the Spanish Government through the Ministerio de Ciencia e Innovacin, the Comunidad de Madrid, and the project i-Math Ingenio Mathematica. This work has been carried out within the framework of the Atlantida project, partially funded by the Spanish Centro para el Desarrollo Tecnolgico e Industrial, in which the Universidad Rey Juan Carlos is collaborating with GVM Aerospace and Defence.

References

[1] M. Soler, A. Olivares, and E. Staffetti. Hybrid optimal control approach to commercial aircraft trajectory optimization. *Journal of Guidance Control and Dynamics*, 33(3):985–991, May-June 2010.

[2] J. Lygeros, S. Sastry, and C.Tomlin. The art of hybrid system. Compendium of Lecture Notes for the Hybrid Systems Class, 2002.

[3] I. Lymperopoulos, A. Lecchini, W. Glover, J. Maciejowski, and J. Lygeros. A stochastic hybrid model for air traffic management processes. *University of Cambridge, Cambridge, CB2 1PZ, UK, Tech. Rep. CUED/F-INFENG/TR*, 572, 2007.

[4] M. S. Branicky, V. S. Borkar, and S. K. Mitter. A unified framework for hybrid control: Model and optimal control theory. *IEEE Transactions on Automatic Control*, 43(1):31–45, 1998.

[5] I.M. Ross and C.N. D'Souza. Hybrid optimal control framework for mission planning. *Journal of Guidance Control and Dynamics*, 28(4):686, 2005.

[6] X. Xu and P. J. Antsaklis. Optimal control of switched systems via nonlinear optimization based on direct differentiations of value functions. *International Journal of Control*, 75(16/17):1406–1426, 2002.

[7] X. Xu and P. J. Antsaklis. Results and perspectives on computational methods for optimal control of switched systems. In *Hybrid Systems: Computation and Control*, pages 540–555. Springer, 2003.

[8] W. Roh and Y. Kim. Trajectory optimization for a multi-stage launch vehicle using time finite element and direct collocation methods. *Engineering Optimization*, 34(1):15–32, 2002.

[9] G.T. Huntington and A.V. Rao. Optimal Configuration of Spacecraft Formations via a Gauss Pseudospectral Method. *Advances in the Astronautical Sciences*, 120:33–50, 2005.

[10] T. R. Jorris and R. G. Cobb. Multiple method 2-d trajectory optimization satisfying waypoints and no-fly zone constraints. *Journal of Guidance, Control, and Dynamics*, 31(3):May–June, 2008.

[11] T. R. Jorris and R. G. Cobb. Three-dimensional trajectory optimization satisfying waypoints and no-fly constraints. *Journal of Guidance, Control, and Dynamics*, 32(2), March-April 2009.

[12] D. Benson. *A Gauss pseudospectral transcription for optimal control*. PhD thesis, Ph. D. Dissertation, Department of Aeronautics and Astronautics, Massachusetts Institute of Technology, 2004.

[13] F. Fahroo and I.M. Ross. Direct trajectory optimization by a Chebyshev pseudospectral method. *Journal of Guidance, Control, and Dynamics*, 25(1):160–166, 2002.

[14] I.M. Ross and F. Fahroo. Pseudospectral knotting methods for solving optimal control problems. *Journal of Guidance, Control, and Dynamics*, 27(3):397–405, 2004.

[15] X. Xu and P. J. Antsaklis. Optimal control of switched systems based on parameterization of the switching instants. *IEEE Transactions on Automatic Control*, 49(1):2–16, 2004.

[16] M. Žefran. *Continuous Methods for Motion Planning*. PhD thesis, University of Pennsylvania, Computer and Information Science, 1996.

[17] C. R. Hargraves and S. W. Paris. Direct trajectory optimization using nonlinear programming and collocation. *Journal of Guidance, Control, and Dynamics*, 10(4):338–342, 1987.

[18] A. L. Herman and B. A. Conway. Direct optimization using collocation based on igh-order gauss-lobatto quadrature rules. *Journal of Guidance, Control, and Dynamics*, 19(3):592–599, May-June 1996.

[19] J. T. Betts and E. J. Cramer. Application of direct transcription to commercial aircraft trajectory optimization. *Journal of Guidance, Control, and Dynamics*, 18(1):151–159, January-February 1995.

[20] D. Wu and Y. J. Zhao. Performances and sensitivities of optimal trajectory generation for air traffic control automation. In AIAA, editor, *Proceedings of 2009 AIAA Guidance, Navigation and Control Conference*. AIAA, 2009.

[21] G. Sachs and T. Christodoulou. Reducing fuel consumption of subsonic aircraft by optimal cyclic cruise. *Journal of Aircraft*, 24(9):616–622, 1987.

[22] P. K. A. Menon. Study of aircraft cruise. *Journal of Guidance, Control and Dynamics*, 15(5):631–639, 1987.

[23] D. M. Pargett and M. D. Ardema. Flight path optimization at constant altitude. *Journal of Guidance Control and Dynamics*, 30(4):1197, 2007.

[24] W. White and J.-P. Clarke. Details and status of cda procedures at los angeles international airport (lax). Presented at CDA Workshop No. 3, Georgia Institute of Technology, Atlanta, GA., September 6-7, 2006.

[25] T. Staigle and G. Nagle. Details and status of cda procedures for early morning arrivals at hartsfield-jackson atlanta international airport (atl),. Presented at CDA Workshop No. 3, Georgia Institute of Technology, Atlanta, GAPresented at CDA Workshop No. 3, Georgia Institute of Technology, Atlanta, GA., September 6-7. 2006.

[26] Ho N. T. Ren L. Brown J. A. Elmer K. R. Tong K.-O. Clarke, J.-P. B. and J. K. Wat. Continuous descent approach: Design and flight test for louisville international airport. *Journal of Aircraft*, 41(5):1054–1066, 2004.

[27] E. Dinges. "determining the environmental benefits of implementing continuous descent approach procedures. In *7th USA/Europe Seminar on Air Traffic Management Research and Development (ATM2009)*, Barcelona, July 2-5 2007.

[28] Mayer R. H. Melby, P. Benefit potential of continuous climb and descent operations. In AIAA, editor, *26th Congress of International Council of Aeronautical Sciences (ICAS)*, Anchorage, AK, Sep. 14-19 2008.

[29] Neskovic D. Shresta, S. and S. S. Williams. Analysis of continuous descent benefits and impacts during daytime operations. In *8th USA/Europe Seminar on Air Traffic Management Research and Development (ATM2009)*, Napa, CA, June 29 - July 2 2009.

[30] Y. Kawajir, C. Laird, and A. Wachter. Introduction to IPOPT: A tutorial for downloading, installing, and using IPOPT, 2006.

[31] A. Nuic. *User Manual for the base of Aircraft Data (BADA) Revision 3.6*. Eurocontrol Experimental Center, 2005.